https://doi.org/10.5194/egusphere-2026-5379
Preprint. Discussion started: 18 September 2026


# Understanding new particle formation based on continuous nanoparticle ranking in boreal forest and urban megacity

Tinghan Zhang[1,2], Wei Du[3], Xinran Zhang[2], Janne Lampilahti[2], Chengfeng Liu[2], Zehao Zou[2], Men Xia[5], Qi Yuan[1], Qiaozhi Zha[5], Jing Cai[7], Yiyang Wang[6], Tom Kokkonen[2], Katrianne Lehtipalo[2,4], Tuukka Petäjä[2], Veli-Matti Kerminen[2], Chao Yan[5], Jingkun Jiang[6], Yongchun Liu[1] and Markku Kulmala[1,2,5]

[1]Aerosol and Haze Laboratory, Beijing Advanced Innovation Center for Soft Matter Science and Engineering, Beijing University of Chemical Technology, Beijing, China
[2]Institute for Atmospheric and Earth System Research/Physics, Faculty of Science, University of Helsinki, Helsinki, Finland
[3]State Key Laboratory of Atmospheric Environment and Extreme Meteorology, Institute of Atmospheric Physics, Chinese Academy of Sciences, Beijing, 100029, China
[4]Atmospheric Composition Research, Finnish Meteorological Institute, Helsinki, Finland
[5]Nanjing-Helsinki Institute in Atmospheric and Earth System Sciences, Nanjing University, Suzhou, China
[6]School of Environment, State Key Joint Laboratory of Environment Simulation and Pollution Control, Tsinghua University, Beijing, China
[7]State Key Laboratory of Climate System Prediction and Risk Management, Nanjing University of Information Science and Technology, Nanjing, 210044, China

*Correspondence to*: duwei@mail.iap.ac.cn, jiangjk@tsinghua.edu.cn

**Abstract.**

Understanding atmospheric new particle formation (NPF) across contrasting environments is essential for evaluating its global-scale impacts. Here, we applied a nanoparticle ranking framework to systematically compare four years (2018–2022) of continuous measurements at the boreal forest site of Hyytiälä and the megacity site of Beijing. Ranking values, as the indicator of the NPF strength, revealed contrasting seasonality: the highest-ranking days occurred mainly in spring in Hyytiälä but in winter in Beijing. The driving factors of NPF in these two distinct environments were then investigated. Unexpectedly, the concentrations of key gaseous precursors, i.e. sulfuric acid (SA) and highly oxygenated organic molecule (HOM) in Hyytiälä and SA in Beijing, did not increase monotonically with the ranking values. Together with the evolution of condensation sink (CS) as a function of ranking values, our results illustrated that NPF intensity is governed by source–sink competition rather than precursor availability alone. Further, we revealed quiet NPF signatures at low ranking values in Hyytiälä, whereas primary anthropogenic emissions obscured such signals in Beijing. The particle formation rate of 7 nm ($J_7$) and growth rates of 7–25 nm ($GR_{7\text{-}25}$) particles were calculated under different ranking levels. The results showed that $J_7$ increased with ranking value, whereas the $GR_{7\text{-}25}$ frequently peaked outside the highest ranking interval. In addition, we also compared the ranking-based $J_7$ and the $J_7$ calculated based on traditional methods, suggesting that conventional approaches may underestimate particle formation during weak or less clearly NPF conditions (low ranking days). By combining

https://doi.org/10.5194/egusphere-2026-5379
Preprint. Discussion started: 18 September 2026


nanoparticle ranking with normalization method, our results continuously and quantitatively characterized NPF dynamics, thereby improving our understanding in the role of NPF in atmospheric aerosol populations in two distinct environments.

## 1 Introduction

Atmospheric new particle formation (NPF) is a multi-stage process initiated by the clustering of gaseous precursors and their subsequent growth into larger aerosol particles (Kulmala et al., 2013). NPF is considered the dominant source of total particle number concentrations in the global atmosphere and can directly influence the Earth's radiative balance as well as human health through the production of ultrafine particles (Gordon et al., 2017; Boucher et al., 2013; Guo et al., 2014; Kulmala et al., 2021; Du et al., 2021; Kulmala et al., 2022a). After their formation, newly formed particles may further grow to larger sizes and eventually exceed the threshold required to act as cloud condensation nuclei (CCN) (Kerminen et al., 2005; Du et al., 2025). Simulations suggest that NPF may contribute up to approximately half of the global CCN population (Merikanto et al., 2009; Dunne et al., 2016; Yu and Luo, 2009; Zhao et al., 2024). Through its influence on CCN abundance, NPF can affect cloud properties, aerosol–cloud interactions, and ultimately the global climate. Therefore, understanding NPF and subsequent particle growth is essential for evaluating the impacts of atmospheric aerosol particles on air quality, climate, and human health.

To elucidate the NPF processes on a global scale, field studies have been conducted worldwide across a wide range of environments, from pristine to heavily polluted area (Kulmala et al., 2004; Kerminen et al., 2018; Chu et al., 2019). In particular, comparative investigations between biogenically and anthropogenically dominated environments are essential for identifying the key NPF mechanisms under different atmospheric conditions and determining whether certain features are universal or site-specific. The Nordic boreal forest has long served as a hotspot for studying NPF in clean environment dominated by biogenic emissions (Kulmala et al., 2012; Kerminen et al., 2018). In this region, NPF is primarily driven by sulfuric acid together with highly oxygenated organic molecules (HOMs) produced from biogenic volatile organic compounds (BVOCs) (Kirkby et al., 2016; Ehn et al., 2014). Owing to the abundant availability of gaseous precursors and low background aerosol loadings, NPF is frequently observed in this region (Dada et al., 2017; Nieminen et al., 2014). Conversely, polluted urban environments are characterized by high pre-existing aerosol concentrations that can strongly suppress the formation of newly formed particles and reduce their survival probability (Du et al., 2022). Nevertheless, intensive NPF events are still frequently observed (Chu et al., 2019; Cai et al., 2017; Yao et al., 2018). Recent studies have demonstrated that NPF in polluted urban area is often dominated by sulfuric acid–amine nucleation, in which anthropogenic amines can efficiently stabilize newly formed clusters even under high condensation sink conditions (Yao et al., 2018; Cai et al., 2020; Yan et al., 2021). Furthermore, the subsequent growth of these particles is promoted by the condensation of sulfuric acid together with oxygenated organic compounds, particularly those originating from anthropogenic volatile organic compounds, which enhances the survival probability of newly formed particles in the polluted urban atmosphere (Qiao et al., 2021; Wang et al., 2020). Beijing, as a typical polluted megacity in China, has therefore become a representative location for investigating NPF under anthropogenic emission dominance.

https://doi.org/10.5194/egusphere-2026-5379
Preprint. Discussion started: 18 September 2026


However, the majority of previous NPF analyses at these two representative regions relied on a binary classification of days to NPF event and non-event days, thus focusing primarily on clearly identifiable, regional-scale NPF events. Such classifications are to some extent influenced by subjective judgment and may overlook the information contained in the days classified as "non-event" or "undefined" (Buenrostro Mazon et al., 2009). Recently, Kulmala et al. (2022b) found that atmospheric NPF can produce a substantial number of particles even on days when no clear NPF event is identified, a phenomenon referred to as quiet NPF. It further led to the suggestion that a paradigm shift is needed in NPF research using field observations in a more statistical and continuous framework to evaluate NPF characteristics (Kulmala et al., 2024).

Motivated by this perspective, this study provides a systematic comparison of NPF in two contrasting atmospheric environments: the biogenically dominated boreal forest site of Hyytiälä and the anthropogenically influenced megacity site of Beijing. Although NPF at both locations has been investigated extensively, direct comparisons based on a continuous analytical framework applied to long-term measurements remain limited. Here, we apply the recently developed nanoparticle ranking method (Aliaga et al., 2023) to four years of continuous measurements from each site during 2018–2022. Unlike traditional binary event classification, this method characterizes NPF on a continuous scale across all measurement days, including periods of weak or quiet NPF. Building on the overview of the two long-term datasets provided by Kulmala et al. (2025), the present study focuses specifically on NPF characteristics and their underlying processes. In particular, we examine (1) differences in the occurrence probability, intensity, and seasonal variability of NPF between Hyytiälä and Beijing; (2) the factors driving and suppressing NPF; and (3) how particle formation and growth rates derived from the ranking-based approach differ from those obtained using traditional event classification. This framework further allows us to distinguish the factors controlling the intensity of particle formation from those governing the subsequent growth of newly formed particles to larger sizes.

## 2 Methods

### 2.1 Measurement sites

This comparative study is based on the long-term, continuous measurements conducted at two SMEAR-type stations (Stations for Measuring Earth surface - Atmosphere Relations). SMEAR II station is located in a boreal forest in Hyytiälä, Finland (61.85° N, 24.28°E; 181 m A.S.L.) and serves as a representative background site for clean environments. Atmospheric emissions in the surrounding area are predominantly biogenic in origin (Hari et al., 2012; Kulmala et al., 2001). More details about this site are provided by Hari et al. (2012). The Aerosol and Haze Laboratory (BUCT/AHL) is situated on the fifth floor of a university building on the west campus of Beijing University of Chemical Technology in Beijing, China (39.94°N, 116.30°E; 20 m A.S.L.). It represents a typical polluted urban environment influenced mainly by anthropogenic emissions such as cooking activities, traffic and other domestic sources (Liu et al., 2020; Kulmala et al., 2021). Detailed description of this station can be found in Zhou et al. (2020).While Hyytiälä observations have been ongoing since 1995, the measurements

https://doi.org/10.5194/egusphere-2026-5379
Preprint. Discussion started: 18 September 2026


in Beijing began in 2018. Consequently, this study utilized the overlapping observation period from 1 March 2018 to 1 March 2022 for comparative analysis.

## 2.2 Instrumentation

In Hyytiälä and Beijing, the particle number size distributions (PNSD) were obtained using different combinations of particle measurement instruments at the two sites. At Hyytiälä, measurements from the Neutral Cluster and Air Ion Spectrometer (NAIS; Airel Ltd; Mirme and Mirme, 2013; Manninen et al., 2016) and the Differential Mobility Particle Sizer (DMPS; Aalto et al., 2001) were combined. At Beijing, measurements from the NAIS, DMPS, and Particle Size Distribution (PSD) system (Liu et al., 2016; Deng et al., 2022) were integrated according to instrument availability during different measurement periods. The combined PNSDs from all instruments were harmonized to an hourly time resolution before subsequent analysis. In Hyytiälä, PNSD between 2.5 and 1000 nm was obtained by combining measurements from the NAIS (≤7 nm) and the DMPS (>7 nm). In Beijing, the PNSD from 2.5 to 840 nm was retrieved by integrating data from the NAIS, DMPS, and the PSD system. Specifically, for periods before 17:00 on 26 February 2019 and during 2021–2022, PNSD data for particles ≤13 nm was obtained from the NAIS, while data for >13 nm were taken from the PSD system. Between 18:00 on 26 February 2019 and the end of 2020, the NAIS still provided data for particles ≤13 nm, whereas the DMPS was used for particles >13 nm. The merging diameters were selected because intercomparisons between instruments showed better agreement between the NAIS and the other instruments at these size ranges, namely around 7 nm in Hyytiälä and around 13 nm in Beijing. Detailed information on the instrument operation and calibration could be found in our previous studies (Yan et al., 2022; Kulmala et al., 2021).

In general, the NAIS measures both PNSD (2.5 – 42 nm) and ion size distribution (0.8 – 42 nm) using two parallel DMAs (differential mobility analyzer) for positive and negative polarities. In ion mode, naturally charged ions are simultaneously measured in the two columns. In the particle mode, the aerosol particles are charged to opposite polarities by corona-needle chargers before classification and electrical detection. The measurement cycle was set to 2 min for both ion and particle mode, and 30 s for the offset mode. The NAIS system operated with a sample flow rate of 30 LPM in Hyytiälä and 27 LPM in Beijing, while the sheath air flow rate was maintained at 60 LPM per DMA at both sites.

The DMPS measures PNSD in the size range of 3–1000 nm in Hyytiälä and 7–840 nm in Beijing. A typical DMPS system consists of a bipolar charger to establish charge equilibrium, a DMA for size classification, and a condensation particle counter (CPC) to obtain the number concentration of particles. The time resolution of the DMPS measurement is 10 min.

In Beijing, the PSD system consists of a nano-scanning mobility particle sizer (nano-SMPS) covering the 3–55 nm range, a long-SMPS covering the 25–650 nm range, and an aerodynamic particle sizer (APS) measuring particles from 0.55 to 10 μm in aerodynamic diameter. In the present study, only PSD data within the 3–840 nm size range were used to ensure consistency with the upper size limit of the Beijing DMPS-based PNSD data. The time resolution of the PSD system data is 5 min.

In addition, the chemical components of gaseous precursors and particulate mass, as well as the meteorological conditions were also obtained at two stations. Sulfur dioxide ($SO_2$) concentrations were measured using Thermo 43i-TLE analyzers in

https://doi.org/10.5194/egusphere-2026-5379
Preprint. Discussion started: 18 September 2026


both Hyytiälä and Beijing. At both sites, the neutral sulfuric acid ($H_2SO_4$), highly oxygenated organic molecules (HOMs), and their clusters were characterized using the time-of-flight chemical ionization mass spectrometers (ToF-CIMS, Aerodyne Research Inc.) (Jokinen et al., 2012) with nitrate ($NO_3^-$) as the reagent ion.

The non-refractory aerosol chemical composition, including organics (Org), sulfate ($SO_4^{2-}$), nitrate ($NO_3^-$), ammonium ($NH_4^+$), and chloride ($Cl^-$), was measured using online aerosol chemical speciation monitors (ACSM; Aerodyne Research Inc.) (Fröhlich et al., 2013). In Beijing, the measurements represented non-refractory fine particulate matter (NR-$PM_{2.5}$), whereas they represented non-refractory submicron aerosol particles (NR-$PM_1$) in Hyytiälä. Hereafter, both measurements are referred to as PM for simplicity.

In Hyytiälä, temperature (T) was measured using a Pt100 sensor inside in a ventilated, custom-built radiation shield, and relative humidity (RH) was measured with a Rotronic MP102H sensor. Ultraviolet-B radiation (UVB, 280–320 nm) was measured using a Solar Light SL501A pyranometer. The boundary layer height (BLH) was derived from HALO Photonics StreamLine LiDAR following the method described in Manninen et al. (2018). In Beijing, meteorological parameters including T, RH, UVB were measured using a weather station (AWS310, Vaisala Inc.). The BLH was measured using a ceilometer (CL51, Vaisala).

## 2.3 Data analysis

### 2.3.1 Traditional event classification

The traditional NPF event classification followed the procedure proposed by Dal Maso et al. (2005) based on visual inspection of the size distribution data from DMPS measurements at Hyytiälä and from DMPS and PSD measurements at Beijing, depending on instrument availability during different measurement periods. The detailed description of the classification criteria can be found in their work. Concisely, the days were categorized into 4 types: (1) NPF event I days, characterized by a clearly discernible "banana-shaped" pattern in the particle number size distribution temporal surface plot, allowing the calculation of particle formation and growth rates; (2) NPF event II days, indicating the presence of NPF activity but lacking sufficiently clear signatures to reliably quantify formation and growth rates; (3) undefined days, for which the occurrence of NPF is ambiguous; and (4) non-event days, showing no evidence of NPF.

### 2.3.2 Nanoparticle ranking method

The nanoparticle ranking method (Aliaga et al., 2023) was used to characterize the NPF at both sites. Compared to the traditional binary classification to event and non-event days, which relies on subjective visual inspection of individual day (Dal Maso et al., 2005), this approach is more time-efficient and objective The method is based on the number concentration of 2.5–5 nm particles ($N_{2.5–5}$) measured by the NAIS, a size range highly sensitive to the occurrence of atmospheric NPF. Although primary sources such as motor vehicles can also directly emit particles smaller than 5 nm, previous research in Beijing has indicated that traffic emissions play a limited role in atmospheric NPF (Yan et al., 2022). Accordingly,

https://doi.org/10.5194/egusphere-2026-5379
Preprint. Discussion started: 18 September 2026


contributions from other particle sources within this size range are assumed to be minor. Following Aliaga et al. (2023), the dataset was first separated by season, and the daily time period showing a pronounced diurnal enhancement in $N_{2.5-5}$ was identified as the active time window. In the original ranking method, the ranking metric is based on the difference in $N_{2.5-5}$ between the active and background time windows. Considering that in urban environment, it tends to overestimate the background concentration due to the influence of traffic emissions, in the present study, we instead used the 90th percentile of $N_{2.5-5}$ within the active time window as the daily peak value for ranking. All measurement days were then ranked according to this metric and assigned a percentile ranking value ranging from 0 to 100 %. On average, high-ranking days are associated with higher probability of NPF and higher particle formation rates, while low-ranking days correspond to the absence of NPF or weak NPF intensity. This automated and statistical method provides probabilistic information about the occurrence and strength of NPF events. Recently, Kulmala et al. (2022b) found that NPF can occur on lower rates also on non-event days that lack clear nucleation and growth pattern in the size distribution — a phenomenon referred to as "quiet NPF." Since this ranking method quantifies NPF across all days, including the days even with low NPF intensity, it is uniquely capable of capturing information during quiet NPF periods (Kulmala et al., 2024).

### 2.3.3 Calculation of condensation sink

The condensation sink (CS), which represents the loss rate of vapor molecules due to condensation onto pre-existing aerosol particles, was calculated using Eq. (1) , as described by Kulmala et al. (2012), using PNSDs obtained from DMPS measurements in Hyytiälä and from DMPS and PSD measurements in Beijing:

$$CS = 2\pi D \sum_{d_p} \beta_{m,d_p} d_p N_{d_p}, \quad (1)$$

where $D$ is the diffusion coefficient of the condensing vapor, $\beta_{m,d_p}$ is transition−regime correction factor, $d_p$ and $N_{d_p}$ represent the geometric mean diameter and particle number concentration in each size bin, respectively. In Hyytiälä, CS was calculated with hygroscopic growth correction (Laakso et al., 2004).

### 2.3.4 Calculation of growth rate and formation rate

The maximum-concentration method was used to calculate the particle growth rate (GR) based on the equation introduced by Kulmala et al. (2012):

$$GR = \frac{dd_p}{dt} = \frac{\Delta d_p}{\Delta t} = \frac{d_{p2} - d_{p1}}{t_2 - t_1}, \quad (2)$$

where the $d_{p1}$ and $d_{p2}$ represent the particle diameters (in nm) at the time $t_1$ and $t_2$, respectively. For calculation, $d_{p1}$ and $d_{p2}$ correspond to the center diameters of the size bin, and $t_1$ and $t_2$ denote the times when the concentration in that size bin reaches its maximum. The particle GR in the size ranges of 3-7, 7-25 nm were calculated using the particle size distribution data at two sites.

https://doi.org/10.5194/egusphere-2026-5379
Preprint. Discussion started: 18 September 2026


The particle formation rate $J_{d_p}$ of diameter $d_p$ is calculated according to the equation given by Kulmala et al. (2012):

$$J_{d_p} = \frac{dN_{d_p}}{dt} + CoagS_{d_p} \times N_{d_p} + \frac{GR}{\Delta d_p} \times N_{d_p}\,, \quad (3)$$

where the first term on the right−hand side represents the time evolution of the particle number concentration in the size ranges from $d_p$ to $d_p + \Delta d_p$. The second term corresponds to the coagulation sink ($CoagS_{d_p}$), which quantifies the loss rate of particles in this size range due to coagulation with larger particles. The third term accounts for the growth of particles out of the corresponding size range. In principle, GR refers to the growth rate at the upper boundary of the size range, $d_p + \Delta d_p$. In practical calculations, GR was represented by the growth rate determined for the corresponding size range from $d_p$ to $d_p + \Delta d_p$. The formation rate of 7 nm particles ($J_7$) was calculated from the particle number size distribution data at both sites using the growth rate in the 7–25 nm size range. It should be noted that Eq. (3) does not fully account for coagulation between newly formed particles, which may contribute to particle losses under conditions of high aerosol loading in urban environments (Cai and Jiang, 2017; Cai et al., 2026).

## 3 Result and discussion

### 3.1 Overview of NPF at Hyytiälä and Beijing

Using the same analytical framework at both sites, we provide a systematic overview of NPF characteristics in Beijing and Hyytiälä based on the recently developed nanoparticle ranking method (see Sect. 2.3.2). The nanoparticle ranking percentage (hereafter referred to as ranking value) ranges from 0 to 100%, with higher values corresponding to stronger nucleation intensity (Aliaga et al., 2023).

The diurnal evolution of particle number size distributions across the five ranking intervals is shown in Fig. 1. A similar ranking-based analysis was presented by Kulmala et al. (2025), but their figure was based on NAIS measurements and was therefore restricted to particle sizes below approximately 40 nm. By extending the analysis to a broader particle size range, the present figure more clearly resolves the emergence and subsequent growth of particle populations.

At both Hyytiälä and Beijing, the characteristic regional NPF pattern, manifested as a clear banana-shaped growth feature, becomes progressively more distinct with increasing ranking value and is particularly evident when the ranking values exceed a threshold of 80%. In Beijing, two pronounced particle modes are consistently observed during the morning and evening rush hours at ranking values below 60% (Fig. 1b, d, and f). These modes indicate a substantial contribution from primary traffic emissions to the urban ultrafine particle population. In contrast, at high ranking values (>80%), newly formed particles emerge around noon and subsequently grow to larger sizes (Fig. 1j). The timing of this growth pattern, outside the main traffic rush hours, suggests that secondary aerosol production driven by photochemical NPF becomes the dominant source of these particles during the periods with a high ranking value. The ability to better distinguish these traffic-related modes and track their subsequent evolution illustrates the additional information gained by extending the analysis beyond the NAIS size range.

https://doi.org/10.5194/egusphere-2026-5379
Preprint. Discussion started: 18 September 2026


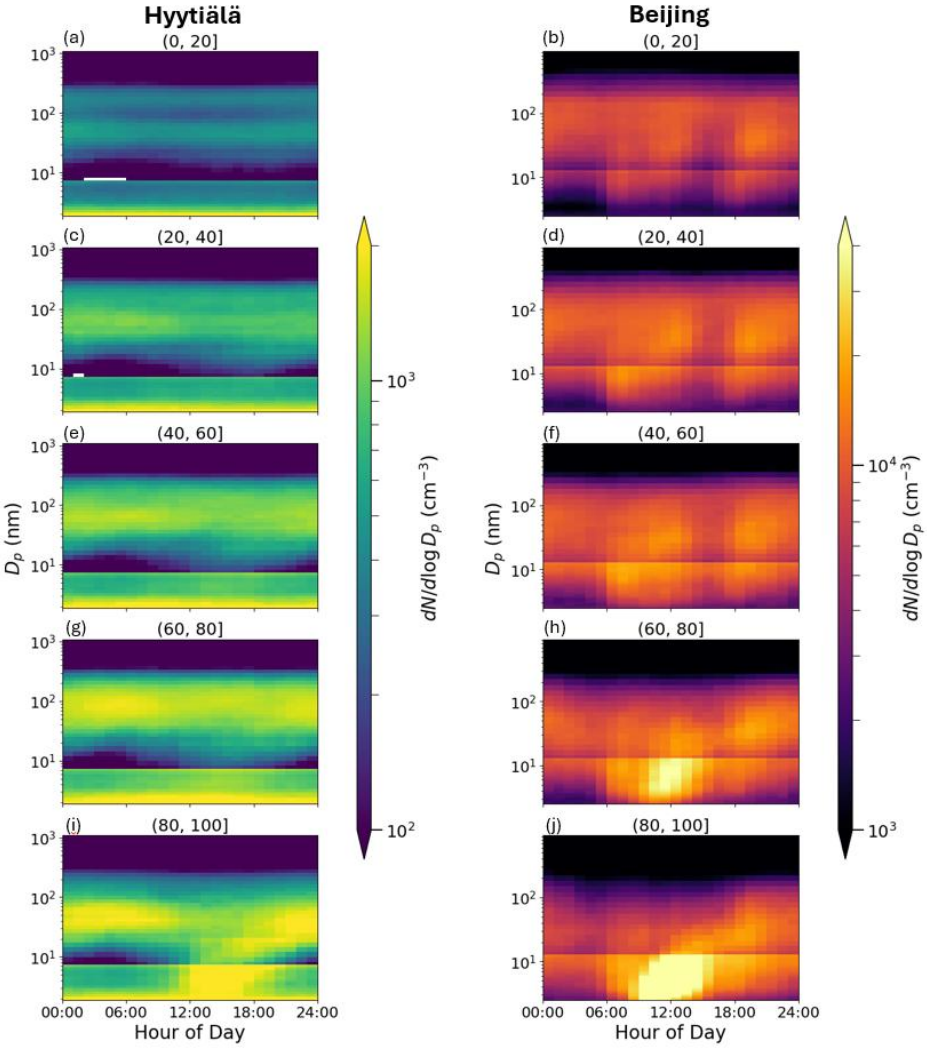


**Figure 1**. Daily median particle number size distributions (PNSDs) grouped into 20 % percentile intervals at Hyytiälä (a, c, e, g, i) and Beijing (b, d, f, h, j). In Hyytiälä, the PNSDs were obtained by combining data from the Neutral Cluster and Air Ion Spectrometer (NAIS, 2.5–7 nm) and the Differential Mobility Particle Sizer (DMPS, 7–1000 nm). In Beijing, the PNSDs were obtained by combining NAIS data for 2.5–13 nm particles with DMPS or PSD data for 13–840 nm particles, depending on instrument availability. The figure is based on hourly median data from 2018 to 2022.

As shown in Fig. 2, the seasonal distribution of ranking values in Hyytiälä and Beijing reflects the seasonal variation of NPF occurrence and intensity at both sites. In Hyytiälä, days with the highest probability and strongest intensity of NPF (ranking values >90%) were mainly concentrated in spring, whereas winter is dominated by days with the lowest NPF potential

https://doi.org/10.5194/egusphere-2026-5379
Preprint. Discussion started: 18 September 2026


(ranking values <10%). This pattern is generally consistent with 16 years long-term observations (Nieminen et al., 2014) in Hyytiälä, which found that NPF events occur most frequently in spring and are rare in winter. In contrast, Beijing exhibited an opposite seasonal pattern. Days with high ranking values (>90%) were most common in winter, suggesting more frequent and intense NPF events during this season, whereas summer was dominated by low-ranking days (<10%), indicating weak or absent NPF events during this period. Deng et al. (2020) similarly reported the highest NPF frequencies in winter and the lowest frequencies in summer. However, based on one year of observations in Beijing in 2004, Wu et al. (2007) found that NPF occurred most frequently in spring, followed by winter and autumn. Likewise, Shang et al. (2023) reported that NPF was most frequent in spring, with winter being the second most active season during 2013–2020 in Beijing. These previous findings indicate a seasonal pattern of NPF activity that differs from that observed in the present study. Such discrepancies may also be associated with long-term changes in Beijing over the past two decades, including the implementation of emission-control policies and rapid urban development. This further highlights the importance of long-term field observations for understanding seasonal variations in NPF intensity. The following section (Sect. 3.2) further elucidates the potential mechanisms underlying these contrasting seasonal behaviors of NPF in the clean Hyytiälä and polluted urban Beijing.

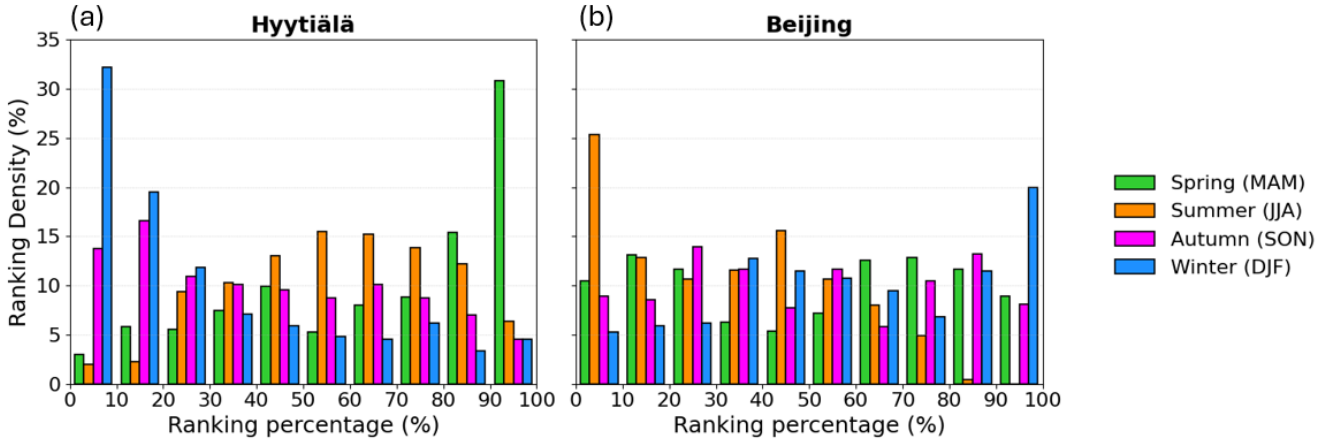


**Figure 2**. Seasonal distribution of percentile ranking in Hyytiälä (a) and Beijing (b) from 2018-2022. Bars show the proportion of days in each 10 % ranking bin for spring (MAM, green), summer (JJA, orange), autumn (SON, magenta), and winter (DJF, blue).

## 3.2 Factors influencing NPF in Hyytiälä and Beijing

### 3.2.1 Gas precursors driving NPF in Hyytiälä and Beijing

The availability of precursor vapors is a key factor driving atmospheric NPF. Previous studies have identified sulfuric acid (SA) as a central precursor for particle formation in both clean and polluted environments, including Hyytiälä and Beijing

https://doi.org/10.5194/egusphere-2026-5379
Preprint. Discussion started: 18 September 2026


(Nieminen et al., 2009; Petäjä et al., 2009; Cai et al., 2021; Yue et al., 2010). Given the important role of precursor vapors in atmospheric nucleation, the precursors would be expected to increase with ranking value at both sites. In Hyytiälä, SA generally increased with ranking value, while declined moderately at the highest-ranking levels in summer (Fig. S1). Considering that highly oxygenated organic molecules (HOMs) also contribute substantially to particle formation and early growth in Hyytiälä (Ehn et al., 2014; Lehtipalo et al., 2018), we therefore examined the product of SA and HOM concentrations. As shown in Figs. 3a – d, the SA × HOM product generally increased with ranking value, but a distinct decrease was still observed at the highest ranking levels (>80%) during spring and summer (Fig. 3a–b). The individual measurements indicate that this decrease was more closely associated with the reduction in HOM concentrations (Fig. S2). Air temperature also decreased at the highest ranking levels during these seasons (Fig. S3), corresponding to the observed reduction in HOM concentrations and the SA × HOM product. Consistently, the temperature coloring in Fig. 3 shows that the decrease in SA × HOM coincided with lower seasonally normalized temperatures. Since biogenic emissions and the subsequent production of HOMs are temperature-dependent, the lower temperatures may reduce the availability of organic vapors and thereby contributed to the decrease in SA × HOM under the most intense NPF conditions. These results suggest that temperature-dependent biogenic vapor production can partly explain the decrease in the SA × HOM product at the highest ranking levels, while the occurrence of the strongest NPF under reduced precursor-vapor availability points to the additional role of other factors, which is examined below through the source–sink balance (Sect. 3.2.3).

In Beijing, SA concentrations generally increased with ranking value, while it remained relatively stable in spring and autumn (Fig. 3e–h). The variation in SA cannot be explained by $SO_2$ abundance alone (Fig. S4), but likely reflects the combined effects of photochemical production, atmospheric mixing, and losses to pre-existing particles. Daytime boundary layer height (BLH) generally increased toward higher ranking values in Beijing (Fig. S5). The development of a deeper daytime boundary layer may be associated with stronger ventilation and more active turbulent mixing, which can dilute pre-existing aerosol particles. Moreover, enhanced boundary-layer development may be associated with stronger daytime photochemistry, as suggested by the generally increasing UVB with BLH at both sites (Fig. S6). This may promote OH production and facilitate $SO_2$ oxidation. Therefore, the variation in SA in Beijing should be interpreted as the combined outcome of $SO_2$ availability, oxidant levels, and meteorological conditions, rather than as a response to $SO_2$ concentration alone.

By characterizing NPF continuously across all measurement days, the ranking method revealed that the dependence of precursor abundance on nucleation intensity differed between the two environments and was not consistently monotonic. Cai et al. (2021) highlighted that the influence of SA on NPF should be considered together with other controlling factors, e.g. amine availability, scavenging by pre-existing aerosols, and so on. These deviations motivated us to further investigate the interplay between precursor sources, particle sinks, and meteorological conditions across seasons (Figs. 4–5).

https://doi.org/10.5194/egusphere-2026-5379
Preprint. Discussion started: 18 September 2026


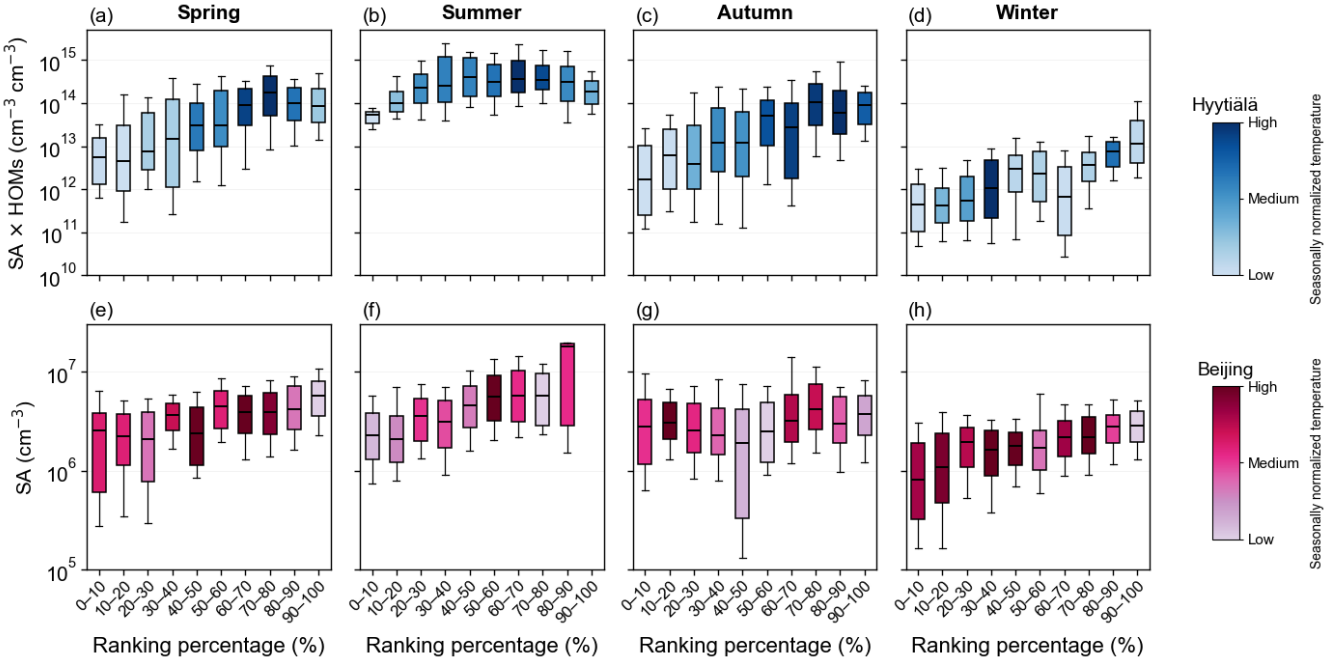


**Figure 3.** Seasonal evolution of sulfuric acid (SA) multiplied by highly oxygenated organic molecules (HOMs) in Hyytiälä (a-d) and SA concentration in Beijing (e-h) as a function of percentile ranking. Each subplot represents one season. The values were calculated from data between 09:00 and 17:00 local time. The boxplots show the median (central line), 25th and 75th percentiles (box edges), and the 10th and 90th percentiles (whiskers). The box colors indicate the corresponding seasonally normalized temperature within each ranking interval, with darker colors representing higher normalized temperatures.

### 3.2.2 Sink suppressing NPF in Hyytiälä and Beijing

The condensation sink (CS) exhibited contrasting ranking dependence at Hyytiälä and Beijing (Fig. 4). In Hyytiälä, CS generally increased from low to intermediate ranking levels but declined at higher ranking values (>80%) across all seasons. A similar non-monotonic pattern was observed for PM mass concentrations, which also increased initially and subsequently decreased toward the highest ranking levels (Fig. S7a-h). Organic aerosol (OA) constituted the dominant fraction of PM in Hyytiälä and showed a similar ranking dependence, indicating that changes in OA contributed substantially to the observed variation in total PM mass. During spring and summer, the decreases in CS and OA at the highest ranking levels also coincided with lower seasonally normalized temperatures (Fig. 4a-b), consistent with the temperature dependence of biogenic emissions. Because PM mass and CS represent different aerosol properties, their co-variation should not be interpreted as a direct equivalence. Nevertheless, the corresponding patterns suggest that changes in the pre-existing aerosol population, particularly the organic aerosol component, may contribute to the non-monotonic dependence of CS on ranking value in Hyytiälä.

https://doi.org/10.5194/egusphere-2026-5379
Preprint. Discussion started: 18 September 2026


In contrast, CS generally decreased with increasing ranking value across all seasons in Beijing. This trend was accompanied by a pronounced decrease in PM mass concentrations (Fig. S7i-p), consistent with the dilution of pre-existing aerosol particles under conditions of enhanced daytime boundary-layer development (Fig. S5). The relative contribution of nitrate to PM also generally decreased toward higher ranking values, whereas the relative contribution of OA increased. It should be noted that the increasing OA fraction does not necessarily indicate an increase in absolute OA mass, as the total PM concentration declined substantially. Previous studies found that $NH_4NO_3$-rich particles can act as efficient sinks for gaseous sulfuric acid in Beijing (Du et al., 2022). Therefore, both the reduction in aerosol loading and the compositional shift away from nitrate-rich particles may contribute to the lower CS at high ranking values, thereby creating more favorable conditions for NPF.

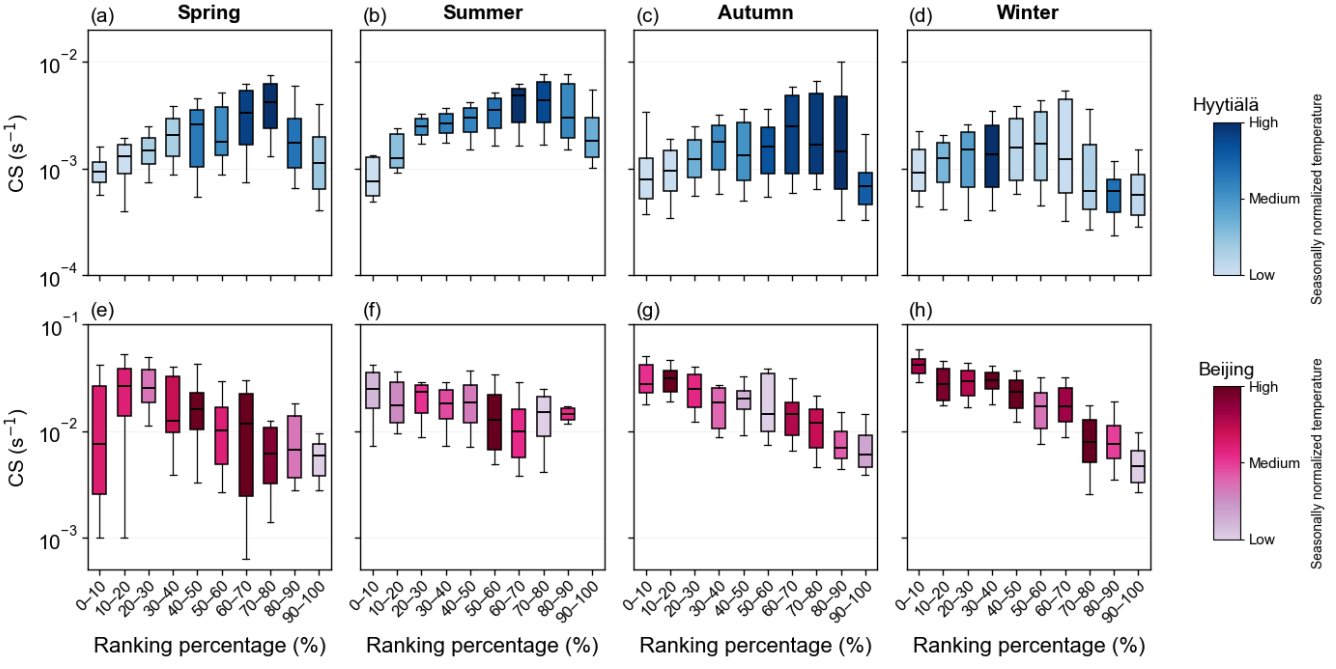


**Figure 4**. Seasonal evolution of condensation sink (a-d) in Hyytiälä and Beijing (e-h) as a function of percentile ranking. Each subplot represents one season. The CS values were calculated from data between 09:00 and 17:00 local time. The boxplots show the median (central line), 25th and 75th percentiles (box edges), and the 10th and 90th percentiles (whiskers). The box colors indicate the corresponding seasonally normalized temperature within each ranking interval, with darker colors representing higher normalized temperatures.

### 3.2.3 Source–Sink Balance Governing NPF in Hyytiälä and Beijing

Figure 5 compares the ranking dependence of the SA × HOM-to-CS ratio at Hyytiälä, together with the SA-to-CS ratio and SA dimer concentration at Beijing. The SA × HOM-to-CS and SA-to-CS ratios serve as simplified source-to-sink proxies,

https://doi.org/10.5194/egusphere-2026-5379
Preprint. Discussion started: 18 September 2026


representing the balance between cluster production and loss to pre-existing aerosol particles, whereas SA dimer concentrations provide a more direct measure of stable molecular clusters available for subsequent growth.

In Hyytiälä, both the SA × HOM and CS decreased at high ranking values (>80%) during spring and summer (Figs. 3 and 4), while the corresponding SA × HOM-to-CS ratio remained relatively high and did not exhibit the same pronounced decline (Fig. 5a–b). This indicates that the concurrent decrease in CS toward the highest ranking levels may partly compensate for the decline in SA × HOM and help sustain conditions favorable for particle formation. Nevertheless, the SA × HOM-to-CS ratio did not increase continuously with ranking value in summer, indicating that this simplified proxy does not capture all processes controlling NPF intensity. In particular, it does not account for the temperature dependence of SA–organic clustering efficiency. Yu et al. (2017) showed that increasing temperature can strongly reduce $H_2SO_4$–organic nucleation rates, with a reduction of approximately 1 order of magnitude for a 10 K temperature increase. The relatively high summer temperatures may alter the efficiency with which available SA and organic vapors contribute to stable cluster formation, thereby weakening the relationship between the SA × HOM-to-CS ratio and nucleation intensity. This temperature dependence may partly explain why the ratio alone does not exhibit a continuous increase with ranking value during summer.

In Beijing, both the SA-to-CS ratios and SA dimer generally increased toward higher ranking values, although the variations were not strictly monotonic across all ranking intervals and seasons (Fig. 5e–l). The increase was particularly pronounced in winter. The similar ranking dependence of these two quantities is physically consistent with the role of SA in initial cluster formation. Whereas the SA-to-CS ratio represents the availability of gaseous SA relative to its loss to pre-existing particles, SA dimers are products of the initial clustering of SA molecules and therefore provide a more direct indication of the molecular clusters available for subsequent growth. Enhanced SA availability relative to CS would be expected to favor both the formation and survival of SA dimers, providing a plausible explanation for the similar trends.

The increases in both variables indicate increasingly favorable source-to-sink conditions toward higher ranking values and may therefore contribute to the stronger NPF intensity observed in Beijing. This relationship is also broadly consistent with the seasonal distribution of ranking values in Beijing (Fig. 2b). Winter was more strongly represented among the highest-ranking days, whereas summer accounted for a larger fraction of the lowest-ranking days. In particular, the pronounced increase in both the SA-to-CS ratios and SA dimer toward high ranking levels in winter indicate increasingly favorable conditions for SA-driven cluster formation and survival during intense NPF events.

Taken together, the patterns at the two sites emphasize that NPF intensity is governed not only by precursor vapor availability, but also by the balance between cluster production and loss. A key consideration is the net availability of clusters that remain after source–sink competition. However, it should be noted that our analysis does not include information on the availability and variation of bases, such as $NH_3$ and amines, which are known to be critical stabilizing vapors for the clustering and early NPF (Lehtipalo et al., 2018; Yao et al., 2018). Therefore, the lack of direct base measurements in the present analysis introduces uncertainty in the quantitative interpretation of cluster formation. Nevertheless, this limitation does not alter the main conclusion that source–sink competition is a key factor regulating the net availability and survival of newly formed clusters.

https://doi.org/10.5194/egusphere-2026-5379
Preprint. Discussion started: 18 September 2026


355

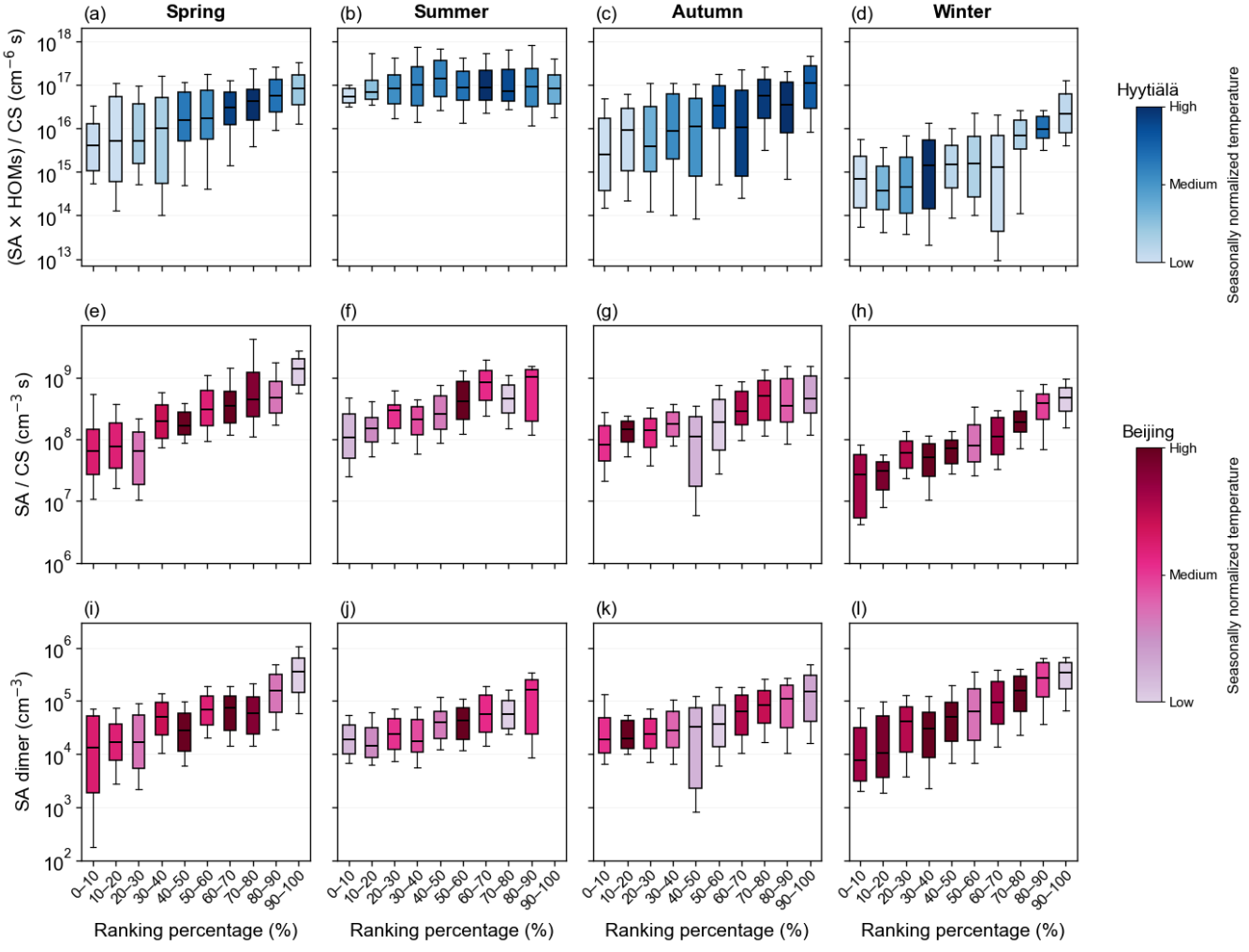


**Figure 5**. Seasonal variation in the ratio of the sulfuric acid (SA) × highly oxygenated organic molecule (HOM) product to the condensation sink (CS) at Hyytiälä (a–d), the ratio of SA concentration to CS in Beijing (e–h), and SA dimer concentration
360 in Beijing (i–l) as a function of percentile ranking. Each subplot represents one season. The values were calculated from data between 09:00 and 17:00 local time. The boxplots show the median (central line), 25th and 75th percentiles (box edges), and the 10th and 90th percentiles (whiskers). The box colors indicate the corresponding air temperature normalized within each season and ranking interval, with darker colors representing higher normalized temperatures.

https://doi.org/10.5194/egusphere-2026-5379
Preprint. Discussion started: 18 September 2026


### 3.3 Particle formation and growth across the NPF intensity spectrum

#### 3.3.1 Quiet NPF at two sites

Similar to Fig. 1, Figure 6 presents the daily evolution of particle PNSDs in Hyytiälä and Beijing across five ranking intervals. However, the PNSDs in Fig. 6 were normalized following the approach proposed by Kulmala et al. (2022b). Specifically, each size bin was scaled to the range of 0–1 based on its minimum and maximum values. Through this normalization, the signals of small-sized particles are no longer overshadowed by the higher concentrations in larger size bins. This normalization allows for the detection of subtle fluctuations in the smallest size channels, thereby facilitating the identification of NPF signatures during "quiet NPF" periods. This improved sensitivity was clearly demonstrated in the normalized PNSDs at the Hyytiälä (Fig. 6a, c, e, g, i). Distinct particle formation and growth patterns were identifiable even when the ranking was below 20%, which was entirely obscured in the raw PNSDs in Hyytiälä in Fig. 1. This finding is consistent with previous observations (Kulmala et al., 2022b), suggesting that NPF processes tend to occur to all the time in the atmosphere. In Beijing (Fig. 6b, d, f, h), a pattern similar to Fig. 1 was observed. Two modes during the morning and evening rush hours remain prominent after normalization when ranking values are below 60%. Due to the influence of anthropogenic primary emissions, the signals of quiet NPF in Beijing are more difficult to isolate and characterize compared to those in Hyytiälä. As an exploratory analysis, the median PNSDs in the 40–60 % interval was divided by those in the 0–20 % interval, based on the simplifying assumption that the lowest-ranking interval was predominantly influenced by traffic emissions. The normalized ratio retains a banana-shaped particle formation and growth pattern (Fig. S8), providing tentative evidence that quiet NPF also occurs in Beijing despite being masked by primary emissions. However, this ratio-based approach relies on the above simplifying assumption and cannot fully separate traffic-related particles from secondary particle formation. Developing methods to accurately identify and track quiet NPF and thereby enable its systematic investigation in polluted urban environments, therefore remains an important task for future research.

After normalization, “banana-shaped” particle growth patterns become evident in PNSDs across all ranking intervals. Based on the temporal evolution of individual size bins, the representative “average” growth rates (GR) for each ranking interval in both Hyytiälä and Beijing were derived by applying the maximum concentration method (see Sect. 2.3.4) to the identified growth features in the normalized PNSDs. Figure S9 illustrates the average GRs for 3–7 nm and 7–25 nm particles in Hyytiälä and Beijing in all ranking intervals. In Beijing, at low ranking values, strong interference from anthropogenic emissions obscures clear growth patterns. Therefore, GR values could only be reliably determined for ranking values above 60%. In Hyytiälä, the average 3 – 7 GRs exhibited a monotonic increase with ranking values, rising from 0.3 nm $h^{-1}$ in the 0–20% interval to 4.4 nm $h^{-1}$ in the 80–100% interval. In contrast, the 3–7 nm GRs in Beijing at high ranking levels (60–80% and 80–100%) were comparable, with values of 3.2 and 3.1 nm $h^{-1}$, respectively. For the 7–25 nm size range, the lowest GR at Hyytiälä was observed in the 0–20% interval (1.9 nm $h^{-1}$). Intriguingly, the GRs in the intermediate ranking intervals (20–80%) were higher (4.2–4.5 nm $h^{-1}$) than those in the highest ranking interval (80–100%, 2.7 nm $h^{-1}$). A similar pattern was observed in Beijing, where the GR in the 60–80% interval (8.1 nm $h^{-1}$) was substantially higher than that in the 80–100%

https://doi.org/10.5194/egusphere-2026-5379
Preprint. Discussion started: 18 September 2026


interval (2.5 nm $h^{-1}$). This phenomenon highlights that in both clean Hyytiälä and polluted Beijing, the growth of 7–25 nm particles does not necessarily peak during the periods of most active NPF. This suggests a potential decoupling between the factors determine the intensity of NPF and those determining particle growth to larger sizes. In both Hyytiälä and Beijing, the decrease in the HOMs concentration at the highest ranking levels during spring and summer (Fig. S2) may also indicate a limitation in the availability of condensable vapors for particle growth under the most intense NPF conditions.

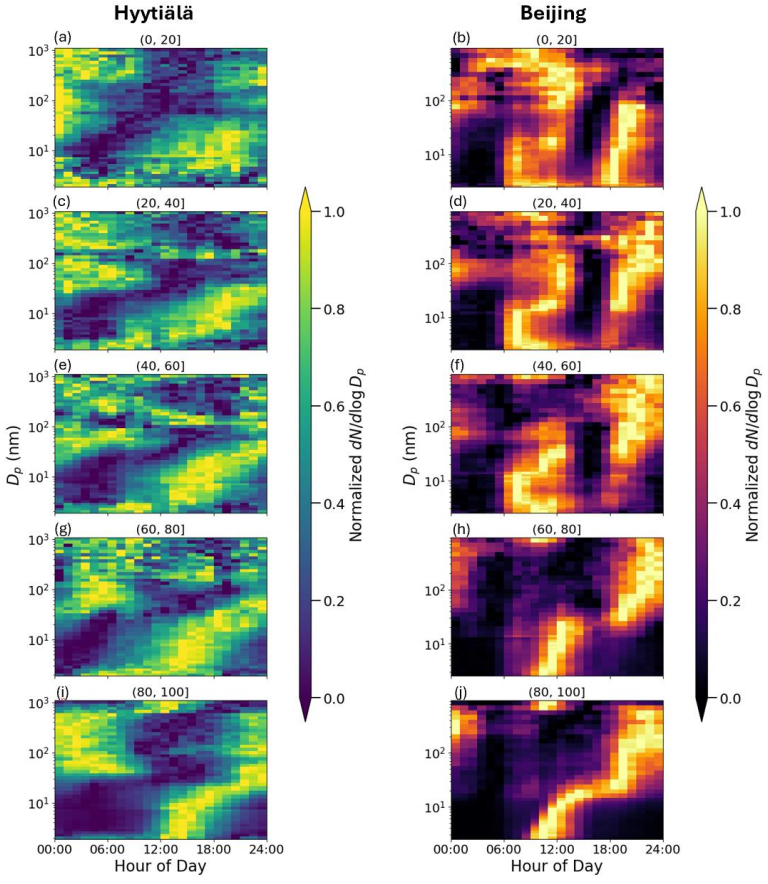


**Figure 6**. Same as Fig. 1, but showing normalized daily median particle number size distributions (PNSDs) grouped into 20 % percentile intervals in Hyytiälä (a, c, e, g, i) and Beijing (b, d, f, h, j) for the period 2018–2022. The PNSDs were normalized such that each size bin was scaled individually to the range of 0–1.

### 3.3.2 Seasonal variation in particle growth rates

Based on the maximum concentration method, we further conducted a seasonal analysis of particle growth in Hyytiälä and Beijing. The average GRs in the 3–7 nm and 7–25 nm size ranges were evaluated across all ranking intervals in Hyytiälä, and for ranking values of 60–100% at Beijing for each season. The fitting procedure and representative clear and uncertain

https://doi.org/10.5194/egusphere-2026-5379
Preprint. Discussion started: 18 September 2026


fitting cases are shown in Figs. S10–S11. Figure 7 presents the seasonal distributions of these average GR values at both sites. In addition, the ranking-based average GRs were compared with traditional event-based GRs calculated using the same maximum concentration method but applied to days traditionally classified as NPF event I days (Sect. 2.3.1) for each season.

In Hyytiälä, the seasonal and ranking dependences differed between the two size ranges. $GR_{3–7}$ was highest in the 80–100 % interval in all seasons and, within this interval, was highest in summer and lowest in autumn (Fig. 7a–d). In contrast, $GR_{7–25}$ showed no consistent increase with ranking value and frequently reached its maximum at intermediate ranking levels, particularly in spring and autumn. The high winter $GR_{7–25}$ values at low ranking levels were associated with uncertain fittings and should be interpreted cautiously.

In Beijing, $GR_{7–25}$ exhibited a clearer seasonal pattern, being highest in summer and lowest in winter in both ranking intervals (Fig. 7e–h). Except in winter, $GR_{7–25}$ was higher in the 60–80 % interval than in the 80–100 % interval. Summer also showed a pronounced enhancement of $GR_{3–7}$ in the highest ranking interval. The ranking-based GRs were generally of similar magnitude to the traditional event-based estimates, although the level of agreement varied by season and size range. Overall, the distinct seasonal and ranking dependences of $GR_{3–7}$ and $GR_{7–25}$, together with the frequent occurrence of the highest $GR_{7–25}$ below the highest ranking interval, indicate that the intensity of initial particle formation and subsequent growth to larger sizes are not necessarily controlled by the same processes.

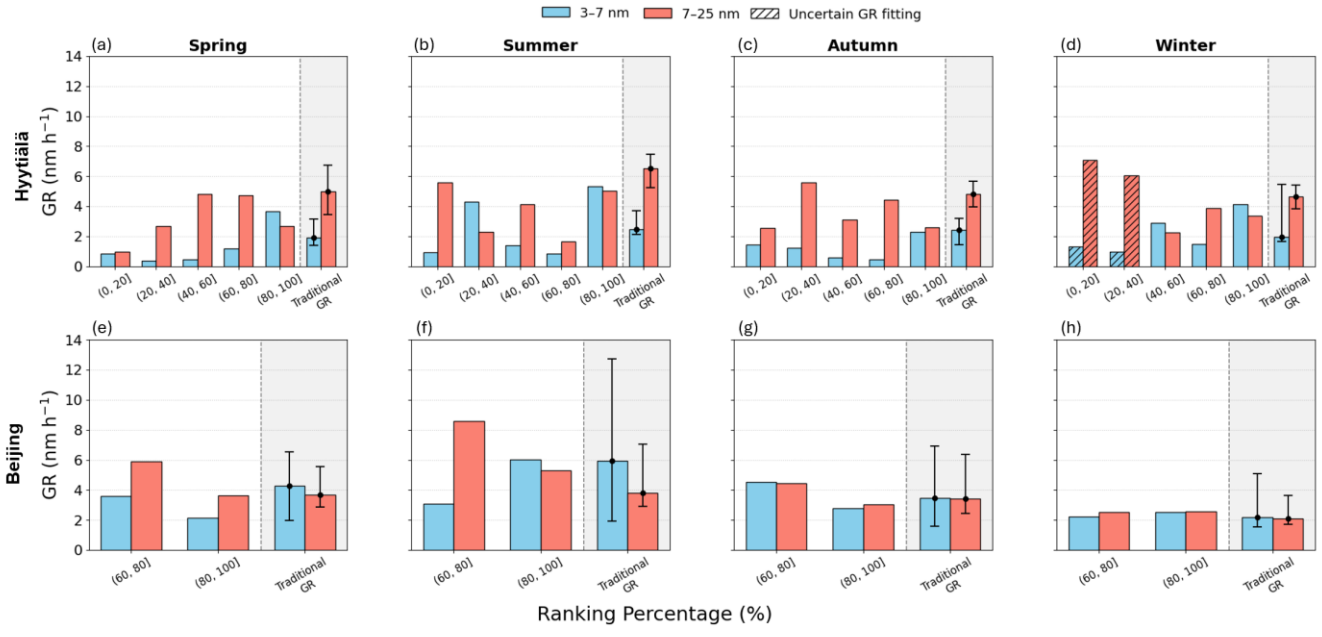


**Figure 7**. Seasonal particle growth rates (GR) for the 3–7 nm (blue bars) and 7–25 nm (red bars) size ranges in Hyytiälä (a–d) and Beijing (e–h). The average GR values were derived using the maximum concentration method (Kulmala et al., 2012) based on averaged normalized particle number size distributions within each percentile ranking interval (see Fig. S3). Bars within

https://doi.org/10.5194/egusphere-2026-5379
Preprint. Discussion started: 18 September 2026


the shaded area represent growth rates derived from days traditionally classified as NPF events using the same maximum concentration method ("traditional GR"). For these bars, the height indicates the median value, and the whiskers represent the 25th and 75th percentiles. Hatched bars indicate cases with higher uncertainty in the growth rate fitting.

### 3.3.3 Particle formation rates at two sites

Using the ranking-based average $GR_{7–25}$ values described above, we calculated a daily ranking-based $J_7$ for each measurement day by assigning the corresponding $GR_{7–25}$ value of its ranking interval. For comparison, we also calculated a daily traditional-method $J_7$ for the same measurement days. In this traditional approach, the corresponding event-based $GR_{7–25}$ values described above were applied to traditionally classified NPF event days. For days without a clearly detectable particle growth signal, the median event-based $GR_{7–25}$ derived from all traditionally classified NPF event days was assigned. The resulting ranking-based and traditional-method $J_7$ values were subsequently grouped according to their ranking intervals, and the median diurnal variations within each interval were compared (Fig. 8).

In line with previous finding (Aliaga et al., 2023), the median $J_7$ values generally increased with ranking value at both Hyytiälä and Beijing, indicating that ranking serves as a reliable proxy for particle formation intensity across contrasting environments. In Hyytiälä, the median ranking based and median traditional-method $J_7$ values were relatively similar in the lowest (0–20%) and highest (80–100%) ranking intervals. However, a clear discrepancy was observed in the intermediate ranking intervals (20–80 %), where the ranking-based $J_7$ was substantially higher than the traditional-method estimate. This difference is consistent with the $GR_{7–25}$ patterns described above. The interval-specific average $GR_{7–25}$ values were relatively high in the intermediate ranking intervals, whereas the traditional calculation assigns a single median event-day $GR_{7–25}$ value to days without a clear particle-growth signal. Consequently, the traditional method may underestimate $J_7$ for a substantial fraction of intermediate-ranking days. This sensitivity highlights the need to better constrain particle growth rates on days that are not captured as conventional NPF events.

The same pattern was also observed in Beijing for the 60–80 % and 80–100 % ranking intervals (Fig. 8f–g), where the difference between ranking-based and traditional-method $J_7$ decreased markedly at higher ranking intervals. However, in Beijing, both the ranking based and traditional-method $J_7$ values were substantially higher than those in Hyytiälä within the same ranking intervals, with the disparity reaching about two orders of magnitude. The substantially higher $J_7$ values in Beijing likely reflect the much stronger availability of nucleating vapors and stabilizing compounds in the polluted urban atmosphere (Cai et al., 2020; Yao et al., 2018). In addition, $J_7$ generally peaked around noon in Beijing but later in the afternoon in Hyytiälä. The earlier peak in Beijing is consistent with rapid daytime photochemical production of sulfuric acid and efficient sulfuric-acid–amine clustering in the urban atmosphere (Cai et al., 2020). In contrast, the later peak in Hyytiälä may reflected the delayed appearance of 7 nm particles after initial cluster formation, together with the sustained afternoon contribution of low-volatility biogenic oxidation products to particle growth (Sulo et al., 2021; Ehn et al., 2014).

At both sites, the ranking-based $J_7$ increased with ranking value and reached its maximum in the highest ranking interval. This differs from the behavior of the average $GR_{7–25}$ values, which peaked instead in the intermediate ranking

https://doi.org/10.5194/egusphere-2026-5379
Preprint. Discussion started: 18 September 2026


intervals (20–80%) at both sites. The observation that the highest particle formation rates do not coincide with the strongest particle growth further supports the interpretation that the mechanisms governing particle formation and subsequent particle growth may be decoupled.

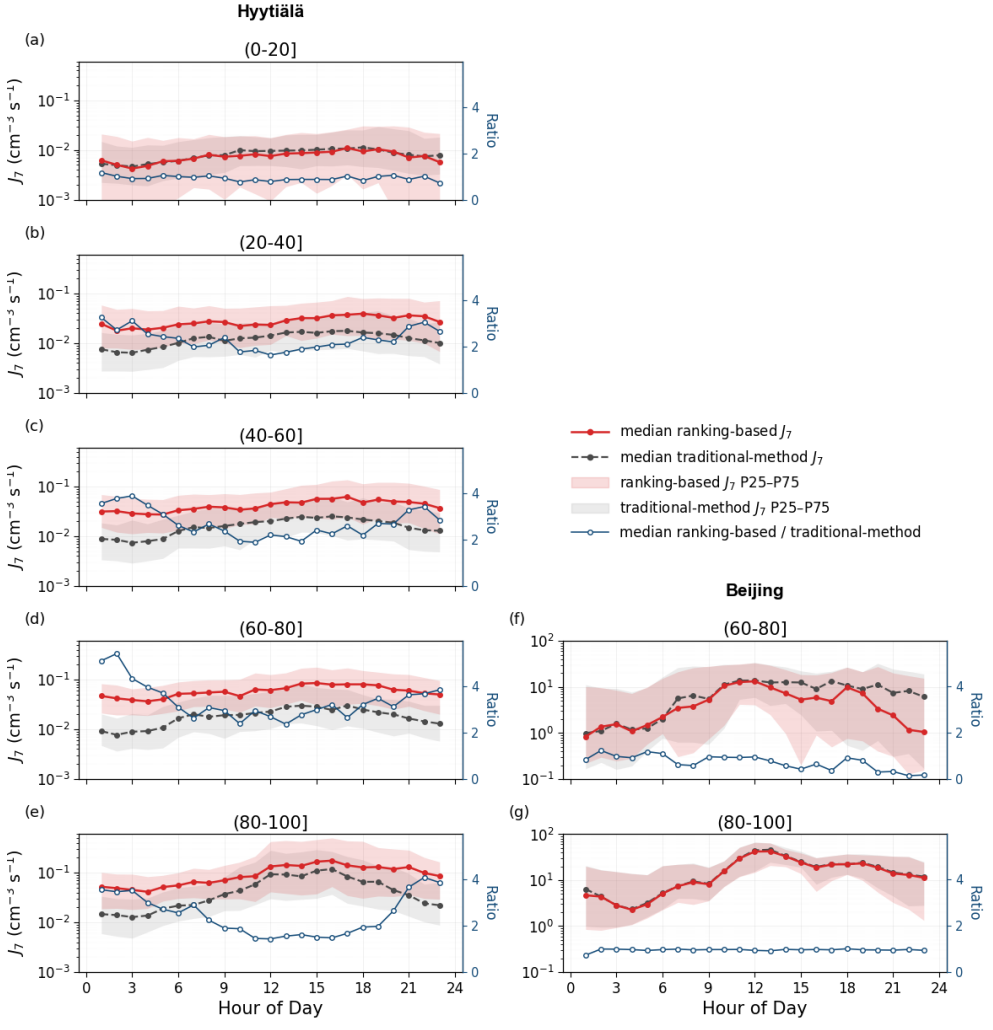


**Figure 8.** Diurnal variation of the formation rate of 7 nm particles ($J_7$) at Hyytiälä (a–e) and Beijing (f–g) for different ranking-percentile intervals during 2018–2022. The red solid lines represent the median ranking-based $J_7$ calculated for all days within each ranking interval using the corresponding interval-specific growth rate of 7–25 nm particles ($GR_{7–25}$). The black dashed lines represent the median $J_7$ calculated using the traditional method for the same days. For traditional classified NPF-event days, event-specific $GR_{7–25}$ values were used, whereas for non-event days, the median $GR_{7–25}$ across all NPF event days was assigned. The red and grey shaded areas indicate the corresponding 25th–75th percentile ranges. The blue lines with open circles show the ratio of the median ranking-based $J_7$ to the median traditional-method $J_7$, plotted on the right-hand axis.

https://doi.org/10.5194/egusphere-2026-5379
Preprint. Discussion started: 18 September 2026


## 4 Summary and conclusions

In this study, we applied a consistent analytical framework to compare the characteristics of NPF in two contrasting environments: the biogenically dominated boreal forest site of Hyytiälä and the anthropogenically influenced megacity site of Beijing. By applying the same nanoparticle ranking framework to four years of continuous measurements from 2018 to 2022, we characterized NPF across the full spectrum of measurement days. Clear banana-shaped particle growth patterns became more evident in the highest ranking intervals. These results demonstrate that the ranking approach provides a robust framework for continuously characterizing the occurrence and intensity of atmospheric NPF in both clean and polluted environments.

The seasonal distributions of ranking values differed markedly between the two environments. In Hyytiälä, the highest-ranking days occurred predominantly in spring, whereas winter was characterized by a large fraction of low-ranking days. In Beijing, high-ranking days were most common in winter, while summer contributed strongly to the lowest-ranking intervals. The factors associated with these seasonal patterns also differed between the two sites. In Hyytiälä, the SA × HOM product generally increased from low to intermediate ranking levels but decreased at the highest ranking levels during spring and summer. However, the simultaneous decrease in the condensation sink (CS) partly compensated for the reduced precursor-vapor availability, allowing the SA × HOM-to-CS ratio to remain relatively high. The ratio did not increase continuously with ranking value in summer, indicating that this simplified proxy does not capture all processes governing NPF intensity, potentially including the temperature dependence of SA–organic clustering. In Beijing, both the SA-to-CS ratios and SA dimer generally increased toward higher ranking values, particularly in winter. The decrease in CS was accompanied by lower PM concentrations and changes in aerosol composition, consistent with increasingly favorable conditions for the survival of newly formed clusters. These findings indicate that NPF intensity cannot be interpreted solely in terms of the abundance of precursor vapors. Instead, an important consideration is the availability of molecular clusters that remain after competition between cluster formation and loss to pre-existing aerosol particles.

Normalization of the particle number size distributions further revealed particle formation and growth signatures that were obscured in the original size distributions, particularly at low ranking values in Hyytiälä. These results suggest that quiet NPF is a common feature of the boreal forest atmosphere. In Beijing, quiet NPF signatures were more difficult to isolate at low ranking values because of the strong influence of primary anthropogenic emissions, especially traffic-related particle modes. Nevertheless, at sufficiently high ranking levels, the normalization approach allowed representative particle growth rates to be determined consistently at both sites.

The ranking-based growth rate analysis also revealed that particle formation intensity and subsequent particle growth do not necessarily vary in parallel. In Hyytiälä, the average growth rates of 3–7 nm particles were highest in the 80–100 % ranking interval in all seasons. In contrast, the growth rates of 7–25 nm particles often reached their maximum in intermediate ranking intervals rather than under the most intense NPF conditions. At both sites, the highest $GR_{7–25}$ values were often observed outside the highest ranking interval. These findings further suggest that the conditions favoring intense particle formation are not necessarily those promoting the fastest subsequent particle growth.

https://doi.org/10.5194/egusphere-2026-5379
Preprint. Discussion started: 18 September 2026


Using the ranking-based growth rates, we calculated the formation rate of 7 nm particles ($J_7$) for all measurement days and compared the results with estimates derived using the traditional approach. At both sites, the median $J_7$ generally increased with ranking value and reached its maximum in the highest ranking interval, supporting the use of ranking value as an indicator of particle formation intensity. However, ranking-based $J_7$ values were higher than the traditional-method $J_7$ in intermediate ranking intervals. This discrepancy suggests that assigning a single median event-day growth rate to days without a clearly detectable particle growth signal may underestimate particle formation rates during weak NPF periods.

Overall, this study demonstrates that a continuous ranking-based framework provides information that is not fully captured by traditional event classification. The results highlight the importance of considering source–sink competition when interpreting NPF intensity and suggest that the factors favoring particle formation are not necessarily identical to those promoting subsequent particle growth. Further efforts to quantify growth rates during weak and quiet NPF periods will be important for evaluating the contribution of continuously occurring particle formation to atmospheric aerosol populations and their potential climatic effects.

**Data availability**

The measurement data from SMEAR II (Hyytiälä) and BUCT/AHL (Beijing), are available from the corresponding authors upon request.

**Author contributions**

MK and WD conceptualized the original idea. TZ performed the data analysis and wrote the paper under the supervision of WD. All authors contributed to the discussion of the results and provided input for the paper.

**Competing interests**

At least one of the (co-)authors is a member of the editorial board of Atmospheric Chemistry and Physics, and the authors also have no other competing interests to declare.

**Acknowledgments**

The technical and scientific staff of the SMEAR II station and the BUCT Atmospheric Haze Laboratory (AHL), as well as all others who contributed to the measurements, are gratefully acknowledged. The authors used ChatGPT (OpenAI) to improve the English language and readability of the manuscript. All AI-assisted text was reviewed and edited by the authors, who take full responsibility for the final content of the manuscript.

**Financial support**

https://doi.org/10.5194/egusphere-2026-5379
Preprint. Discussion started: 18 September 2026


This work has been supported by the ACCC Flagship funded by the Research Council of Finland (grant nos. 337549), Research Council of Finland project (grant nos. 316114, 325647, 325681 and 347782), the "Gigacity" project funded by the Jenny and Antti Wihuri Foundation, and the National Natural Science Foundation of China (grant nos. 42175113).

## References

Aalto, P., Hämeri, K., Becker, E., Weber, R., Salm, J., Mäkelä, J. M., Hoell, C., O'dowd, C. D., Hansson, H.-C., and Väkevä, M.: Physical characterization of aerosol particles during nucleation events, Tellus B: Chemical and Physical Meteorology, 53, 344-358, 2001.

Aliaga, D., Tuovinen, S., Zhang, T., Lampilahti, J., Li, X., Ahonen, L., Kokkonen, T., Nieminen, T., Hakala, S., and Paasonen, P.: Nanoparticle ranking analysis: determining new particle formation (NPF) event occurrence and intensity based on the concentration spectrum of formed (sub-5 nm) particles, Aerosol Research, 1, 81-92, 2023.

Boucher, O., Randall, D., Artaxo, P., Bretherton, C., Feingold, G., Forster, P., Kerminen, V.-M., Kondo, Y., Liao, H., and Lohmann, U.: Clouds and aerosols, in: Climate change 2013: The physical science basis. Contribution of working group I to the fifth assessment report of the intergovernmental panel on climate change, Cambridge University Press, 571-6572013.

Buenrostro Mazon, S., Riipinen, I., Schultz, D., Valtanen, M., Dal Maso, M., Sogacheva, L., Junninen, H., Nieminen, T., Kerminen, V.-M., and Kulmala, M.: Classifying previously undefined days from eleven years of aerosol-particle-size distribution data from the SMEAR II station, Hyytiälä, Finland, Atmospheric Chemistry and Physics, 9, 667-676, 2009.

Cai, R. and Jiang, J.: A new balance formula to estimate new particle formation rate: reevaluating the effect of coagulation scavenging, Atmospheric Chemistry and Physics, 17, 12659-12675, 2017.

Cai, R., Yang, D., Fu, Y., Wang, X., Li, X., Ma, Y., Hao, J., Zheng, J., and Jiang, J.: Aerosol surface area concentration: a governing factor in new particle formation in Beijing, Atmospheric Chemistry and Physics, 17, 12327-12340, 2017.

Cai, R., Li, X., Yin, R., Zhao, B., Yan, C., Kangasluoma, J., Zhang, X., Zheng, J., Xie, H.-B., and Kerminen, V.-M.: New Particle Formation and Growth in Urban Atmospheres: From Observations to Molecular-Level Understanding, Chemical reviews, 2026.

Cai, R., Yan, C., Worsnop, D. R., Bianchi, F., Kerminen, V.-M., Liu, Y., Wang, L., Zheng, J., Kulmala, M., and Jiang, J.: An indicator for sulfuric acid–amine nucleation in atmospheric environments, Aerosol Science and Technology, 55, 1059-1069, 2021.

Cai, R., Yan, C., Yang, D., Yin, R., Lu, Y., Deng, C., Fu, Y., Ruan, J., Li, X., and Kontkanen, J.: Sulfuric acid-amine nucleation in urban Beijing, Atmospheric Chemistry and Physics Discussions, 2020, 1-19, 2020.

Chu, B., Kerminen, V.-M., Bianchi, F., Yan, C., Petäjä, T., and Kulmala, M.: Atmospheric new particle formation in China, Atmospheric Chemistry and Physics, 19, 115-138, 2019.

Dada, L., Paasonen, P., Nieminen, T., Buenrostro Mazon, S., Kontkanen, J., Peräkylä, O., Lehtipalo, K., Hussein, T., Petäjä, T., and Kerminen, V.-M.: Long-term analysis of clear-sky new particle formation events and nonevents in Hyytiälä, Atmospheric Chemistry and Physics, 17, 6227-6241, 2017.

Dal Maso, M., Kulmala, M., Riipinen, I., Wagner, R., Hussein, T., Aalto, P. P., and Lehtinen, K. E.: Formation and growth of fresh atmospheric aerosols: eight years of aerosol size distribution data from SMEAR II, Hyytiälä, Finland, Boreal environment research, 10, 323, 2005.

Deng, C., Fu, Y., Dada, L., Yan, C., Cai, R., Yang, D., Zhou, Y., Yin, R., Lu, Y., and Li, X.: Seasonal characteristics of new particle formation and growth in urban Beijing, Environmental science & technology, 54, 8547-8557, 2020.

Deng, C., Li, Y., Yan, C., Wu, J., Cai, R., Wang, D., Liu, Y., Kangasluoma, J., Kerminen, V.-M., and Kulmala, M.: Measurement report: Size distributions of urban aerosols down to 1 nm from long-term measurements, Atmospheric Chemistry and Physics, 22, 13569-13580, 2022.

Du, W., Cai, J., Zheng, F., Yan, C., Zhou, Y., Guo, Y., Chu, B., Yao, L., Heikkinen, L. M., and Fan, X.: Influence of aerosol chemical composition on condensation sink efficiency and new particle formation in beijing, Environmental science & technology letters, 9, 375-382, 2022.

Du, W., Dada, L., Zhao, J., Chen, X., Daellenbach, K. R., Xie, C., Wang, W., He, Y., Cai, J., and Yao, L.: A 3D study on the amplification of regional haze and particle growth by local emissions, npj Climate and Atmospheric Science, 4, 4, 2021.

https://doi.org/10.5194/egusphere-2026-5379
Preprint. Discussion started: 18 September 2026


Du, W., Zhao, J., Dada, L., Xu, W., Wang, Y., Shi, Y., Chen, X., Kokkonen, T. V., Cai, J., and Zhang, Y.: Impacts of enhanced new-particle growth events above urban roughness sublayer on cloud condensation nuclei, One Earth, 8, 2025.
Dunne, E. M., Gordon, H., Kürten, A., Almeida, J., Duplissy, J., Williamson, C., Ortega, I. K., Pringle, K. J., Adamov, A., and Baltensperger, U.: Global atmospheric particle formation from CERN CLOUD measurements, Science, 354, 1119-1124, 2016.
Ehn, M., Thornton, J. A., Kleist, E., Sipilä, M., Junninen, H., Pullinen, I., Springer, M., Rubach, F., Tillmann, R., and Lee, B.: A large source of low-volatility secondary organic aerosol, Nature, 506, 476-479, 2014.
Fröhlich, R., Cubison, M., Slowik, J., Bukowiecki, N., Prévôt, A., Baltensperger, U., Schneider, J., Kimmel, J., Gonin, M., and Rohner, U.: The ToF-ACSM: a portable aerosol chemical speciation monitor with TOFMS detection, Atmospheric Measurement Techniques, 6, 3225-3241, 2013.
Gordon, H., Kirkby, J., Baltensperger, U., Bianchi, F., Breitenlechner, M., Curtius, J., Dias, A., Dommen, J., Donahue, N. M., and Dunne, E. M.: Causes and importance of new particle formation in the present-day and preindustrial atmospheres, Journal of Geophysical Research: Atmospheres, 122, 8739-8760, 2017.
Guo, S., Hu, M., Zamora, M. L., Peng, J., Shang, D., Zheng, J., Du, Z., Wu, Z., Shao, M., and Zeng, L.: Elucidating severe urban haze formation in China, Proceedings of the National Academy of Sciences, 111, 17373-17378, 2014.
Hari, P., Nikinmaa, E., Pohja, T., Siivola, E., Bäck, J., Vesala, T., and Kulmala, M.: Station for measuring ecosystem-atmosphere relations: SMEAR, in: Physical and physiological forest ecology, Springer, 471-4872012.
Jokinen, T., Sipilä, M., Junninen, H., Ehn, M., Lönn, G., Hakala, J., Petäjä, T., Mauldin Iii, R., Kulmala, M., and Worsnop, D.: Atmospheric sulphuric acid and neutral cluster measurements using CI-APi-TOF, Atmospheric Chemistry and Physics, 12, 4117-4125, 2012.
Kerminen, V.-M., Chen, X., Vakkari, V., Petäjä, T., Kulmala, M., and Bianchi, F.: Atmospheric new particle formation and growth: review of field observations, Environmental Research Letters, 13, 103003, 2018.
Kerminen, V. M., Lihavainen, H., Komppula, M., Viisanen, Y., and Kulmala, M.: Direct observational evidence linking atmospheric aerosol formation and cloud droplet activation, Geophysical research letters, 32, 2005.
Kirkby, J., Duplissy, J., Sengupta, K., Frege, C., Gordon, H., Williamson, C., Heinritzi, M., Simon, M., Yan, C., and Almeida, J.: Ion-induced nucleation of pure biogenic particles, Nature, 533, 521-526, 2016.
Kulmala, M., Vehkamäki, H., Petäjä, T., Dal Maso, M., Lauri, A., Kerminen, V.-M., Birmili, W., and McMurry, P.: Formation and growth rates of ultrafine atmospheric particles: a review of observations, Journal of Aerosol Science, 35, 143-176, 2004.
Kulmala, M., Aliaga, D., Tuovinen, S., Cai, R., Junninen, H., Yan, C., Bianchi, F., Cheng, Y., Ding, A., and Worsnop, D. R.: Opinion: A paradigm shift in investigating the general characteristics of atmospheric new particle formation using field observations, Aerosol Research, 2, 49-58, 2024.
Kulmala, M., Cai, R., Stolzenburg, D., Zhou, Y., Dada, L., Guo, Y., Yan, C., Petäjä, T., Jiang, J., and Kerminen, V.-M.: The contribution of new particle formation and subsequent growth to haze formation, Environmental Science: Atmospheres, 2, 352-361, 2022a.
Kulmala, M., Dada, L., Daellenbach, K. R., Yan, C., Stolzenburg, D., Kontkanen, J., Ezhova, E., Hakala, S., Tuovinen, S., and Kokkonen, T. V.: Is reducing new particle formation a plausible solution to mitigate particulate air pollution in Beijing and other Chinese megacities?, Faraday Discussions, 226, 334-347, 2021.
KULMALA, M., HÄMERI, K., Aalto, P., Mäkelä, J., PIRJOLA, L., Nilsson, E. D., Buzorius, G., Rannik, Ü., Maso, M. D., and Seidl, W.: Overview of the international project on biogenic aerosol formation in the boreal forest (BIOFOR), Tellus B, 53, 324-343, 2001.
Kulmala, M., Junninen, H., Dada, L., Salma, I., Weidinger, T., Thén, W., Vörösmarty, M., Komsaare, K., Stolzenburg, D., and Cai, R.: Quiet new particle formation in the atmosphere, Frontiers in Environmental Science, 10, 912385, 2022b.
Kulmala, M., Kontkanen, J., Junninen, H., Lehtipalo, K., Manninen, H. E., Nieminen, T., Petäjä, T., Sipilä, M., Schobesberger, S., and Rantala, P.: Direct observations of atmospheric aerosol nucleation, Science, 339, 943-946, 2013.
Kulmala, M., Petäjä, T., Nieminen, T., Sipilä, M., Manninen, H. E., Lehtipalo, K., Dal Maso, M., Aalto, P. P., Junninen, H., and Paasonen, P.: Measurement of the nucleation of atmospheric aerosol particles, Nature protocols, 7, 1651-1667, 2012.
Kulmala, M., Wei, D., Zhang, X., Zhang, T., Xia, M., Wang, Y., Zou, Z., Zheng, F., Zhang, Y., and Yang, C.: Understanding atmospheric processes: insights from the comparison between Beijing and Hyytiälä, Npj Clean Air, 1, 26, 2025.
Laakso, L., Petäjä, T., Lehtinen, K. E., Kulmala, M., Paatero, J., Horrak, U., Tammet, H., and Joutsensaari, J.: Ion production rate in a boreal forest based on ion, particle and radiation measurements, Atmospheric Chemistry and Physics, 4, 1933-1943, 2004.

https://doi.org/10.5194/egusphere-2026-5379
Preprint. Discussion started: 18 September 2026


Lehtipalo, K., Yan, C., Dada, L., Bianchi, F., Xiao, M., Wagner, R., Stolzenburg, D., Ahonen, L. R., Amorim, A., and Baccarini, A.: Multicomponent new particle formation from sulfuric acid, ammonia, and biogenic vapors, Science advances, 4, eaau5363, 2018.

Liu, J., Jiang, J., Zhang, Q., Deng, J., and Hao, J.: A spectrometer for measuring particle size distributions in the range of 3 nm to 10 μm, Frontiers of Environmental Science & Engineering, 10, 63-72, 2016.

Liu, Y., Yan, C., Feng, Z., Zheng, F., Fan, X., Zhang, Y., Li, C., Zhou, Y., Lin, Z., and Guo, Y.: Continuous and comprehensive atmospheric observations in Beijing: a station to understand the complex urban atmospheric environment, Big Earth Data, 4, 295-321, 2020.

Manninen, A., Marke, T., Tuononen, M., and O'Connor, E.: Atmospheric boundary layer classification with Doppler lidar, Journal of Geophysical Research: Atmospheres, 123, 8172-8189, 2018.

Manninen, H. E., Mirme, S., Mirme, A., Petäjä, T., and Kulmala, M.: How to reliably detect molecular clusters and nucleation mode particles with Neutral cluster and Air Ion Spectrometer (NAIS), Atmospheric Measurement Techniques, 9, 3577-3605, 2016.

Merikanto, J., Spracklen, D., Mann, G., Pickering, S., and Carslaw, K.: Impact of nucleation on global CCN, Atmospheric Chemistry and Physics, 9, 8601-8616, 2009.

Mirme, S. and Mirme, A.: The mathematical principles and design of the NAIS–a spectrometer for the measurement of cluster ion and nanometer aerosol size distributions, Atmospheric Measurement Techniques, 6, 1061-1071, 2013.

Nieminen, T., Asmi, A., Dal Maso, M., Aalto, P. P., Keronen, P., Petäjä, T., and Kulmala, M.: Trends in atmospheric new-particle formation: 16 years of observations in a boreal-forest environment, Boreal Environment Research, 19, 191, 2014.

Nieminen, T., Manninen, H. E., Sihto, S.-L., Yli-Juuti, T., Mauldin, I., RL, Petaja, T., Riipinen, I., Kerminen, V.-M., and Kulmala, M.: Connection of sulfuric acid to atmospheric nucleation in boreal forest, Environmental science & technology, 43, 4715-4721, 2009.

Petäjä, T., Mauldin, I., RL, Kosciuch, E., McGrath, J., Nieminen, T., Paasonen, P., Boy, M., Adamov, A., Kotiaho, T., and Kulmala, M.: Sulfuric acid and OH concentrations in a boreal forest site, Atmospheric Chemistry and Physics, 9, 7435-7448, 2009.

Qiao, X., Yan, C., Li, X., Guo, Y., Yin, R., Deng, C., Li, C., Nie, W., Wang, M., and Cai, R.: Contribution of atmospheric oxygenated organic compounds to particle growth in an urban environment, Environmental science & technology, 55, 13646-13656, 2021.

Shang, D., Hu, M., Tang, L., Fang, X., Chen, S., Zeng, L., Guo, S., Zhang, Y., and Wu, Z.: New particle formation occurrence in the urban atmosphere of Beijing during 2013–2020, Journal of Geophysical Research: Atmospheres, 128, e2022JD038334, 2023.

Sulo, J., Sarnela, N., Kontkanen, J., Ahonen, L., Paasonen, P., Laurila, T., Jokinen, T., Kangasluoma, J., Junninen, H., and Sipilä, M.: Long-term measurement of sub-3 nm particles and their precursor gases in the boreal forest, Atmospheric Chemistry and Physics, 21, 695-715, 2021.

Wang, M., Kong, W., Marten, R., He, X.-C., Chen, D., Pfeifer, J., Heitto, A., Kontkanen, J., Dada, L., and Kürten, A.: Rapid growth of new atmospheric particles by nitric acid and ammonia condensation, Nature, 581, 184-189, 2020.

Wu, Z., Hu, M., Liu, S., Wehner, B., Bauer, S., Ma ßLing, A., Wiedensohler, A., Petäjä, T., Dal Maso, M., and Kulmala, M.: New particle formation in Beijing, China: Statistical analysis of a 1-year data set, Journal of Geophysical Research: Atmospheres, 112, 2007.

Yan, C., Shen, Y., Stolzenburg, D., Dada, L., Qi, X., Hakala, S., Sundström, A.-M., Guo, Y., Lipponen, A., and Kokkonen, T.: The effect of COVID-19 restrictions on atmospheric new particle formation in Beijing, Atmospheric Chemistry and Physics Discussions, 2022, 1-24, 2022.

Yan, C., Yin, R., Lu, Y., Dada, L., Yang, D., Fu, Y., Kontkanen, J., Deng, C., Garmash, O., and Ruan, J.: The synergistic role of sulfuric acid, bases, and oxidized organics governing new-particle formation in Beijing, Geophysical Research Letters, 48, e2020GL091944, 2021.

Yao, L., Garmash, O., Bianchi, F., Zheng, J., Yan, C., Kontkanen, J., Junninen, H., Mazon, S. B., Ehn, M., and Paasonen, P.: Atmospheric new particle formation from sulfuric acid and amines in a Chinese megacity, Science, 361, 278-281, 2018.

Yu, F. and Luo, G.: Simulation of particle size distribution with a global aerosol model: contribution of nucleation to aerosol and CCN number concentrations, Atmospheric Chemistry and Physics, 9, 7691-7710, 2009.

https://doi.org/10.5194/egusphere-2026-5379
Preprint. Discussion started: 18 September 2026


Yu, F., Luo, G., Nadykto, A. B., and Herb, J.: Impact of temperature dependence on the possible contribution of organics to new particle formation in the atmosphere, Atmospheric Chemistry and Physics, 17, 4997-5005, 2017.
Yue, D., Hu, M., Zhang, R., Wang, Z., Zheng, J., Wu, Z., Wiedensohler, A., He, L., Huang, X., and Zhu, T.: The roles of sulfuric acid in new particle formation and growth in the mega-city of Beijing, Atmospheric Chemistry and Physics, 10, 4953-4960, 2010.
Zhao, B., Donahue, N. M., Zhang, K., Mao, L., Shrivastava, M., Ma, P.-L., Shen, J., Wang, S., Sun, J., and Gordon, H.: Global variability in atmospheric new particle formation mechanisms, Nature, 631, 98-105, 2024.
Zhou, Y., Dada, L., Liu, Y., Fu, Y., Kangasluoma, J., Chan, T., Yan, C., Chu, B., Daellenbach, K. R., and Bianchi, F.: Variation of size-segregated particle number concentrations in wintertime Beijing, Atmospheric Chemistry and Physics, 20, 1201-1216, 2020.